Supporting information

Experimental section

Materials

All the commercial materials were used as received without further purification. Lead (II) iodide (PbI_2) were purchased from TCI (Japan). Lead (II) chloride ($PbCl_2$), bathocuproine (BCP) and C60 were purchased from Xi'an Yuri Solar Co., Ltd. Indium tin oxide glass (ITO), methylammonium iodide (MAI) and formamidinium iodide (FAI) were purchased from Advanced Election Technology CO., Ltd (China). 2,3,5,6-Tetrafluoro-7,7,8,8-tetracyanoquinodimethane (F4TCNQ) was purchased from Macklin. 7,7,8,8-Tetracyanoquinodimethane (TCNQ) was purchased from Aladdin. Toluene, chlorobenzene (CB), N, N-dimethylformamide (DMF) and dimethyl sulfoxide (DMSO) were purchased from Sigma-Aldrich (USA). Isopropanol (IPA) was purchased from Energy Chemical.

Preparation of precursors

The TCNQ solution was prepared by dissolving 8 mg TCNQ in 1mL DMF/DMSO (v/v=9:1).

The F4TCNQ solution was prepared by dissolving 8 mg F4TCNQ in 1mL DMF/DMSO (v/v=9:1).

The $(FA_{0.17}MA_{0.94}PbI_{3.11})_{0.95}(PbCl_2)_{0.05}$ perovskite precursor solution was prepared by dissolving 34.4 mg FAI, 36.2 mg $PbCl_2$, 174.9 mg MAI and 539.4 mg PbI_2 in 1mL DMF/DMSO (v/v=9:1).

The TCNQ-doped perovskite precursor solution was prepared by mixing the aforementioned TCNQ solution and $(FA_{0.17}MA_{0.94}PbI_{3.11})_{0.95}(PbCl_2)_{0.05}$ perovskite precursor solution together with different volume ratios, for example volume (perovskite solution): volume (TCNQ solution)=100:0, 95:5, 92.5:7.5, 90:10.

The F4TCNQ-doped perovskite precursor solution was prepared in the same way as the TCNQ-doped perovskite.

All the solutions have been completely dissolved before use.

Devices fabrication

The ITO glass was cleaned by sequentially sonication with glass cleaning fluid, deionized water, acetone and IPA, respectively. After being dried by nitrogen flow, the ITO were treated by UV-Ozone for 15 minutes before use. In glovebox, the perovskite films with or without molecule were formed on ITO by spin-coating at 500 rpm for 3 s, 5000rpm for 27 s, and 150 μL CB was dropped on the spinning substrate at 8 s after the start of the second spin-coating procedure. The resulting substrates were heated on hot plate at 60℃for 1 min, 100℃ for 10 min. Afterward, 20 nm C60 were deposited on the top of perovskite layers via thermal evaporation process at vacuum condition (~3 $\times 10^{-5} Pa$). After this process, the BCP solution of 0.5 mg/mL in IPA was spin coated on C60 film at 5000 rpm for 30s. Finally, 80 nm Ag electrodes were thermally evaporated on the as-prepared film at high vacuum (~3 $\times 10^{-5} Pa$).

Characterizations

The FTIR spectra were recorded by Fourier transform infrared spectroscopy (Nicolet is10) under illumination of 500W LED. The XRD pattern were analyzed by Bruker-axs XRD with a Cu Kα radiation source. The UV-vis absorption spectra were measured by ultraviolet visible (UV-vis) spectroscopy (Shimadzu UV-2500). Steady-state photoluminescence (PL) spectra and time-resolved PL (TRPL) spectra were obtained by FLS1000 (Edinburgh instruments). The PL mapping images were obtained via Vis-NIR-XU (Nanophoto corporation). The KPFM and AFM were measured by Cypher ES (Oxford Instruments Asylum Research). The SEM images were characterized by S7-70 (Japan Hitachi Nake High-Tech Enterprise). The space charge limiting current (SCLC), Mott-Schottky analysis and electrochemical impedance (EIS) were performed in the dark by electrochemical workstation (CHI660, China). The J-V characteristics of PSCs were performed in glove box under AM 1.5 G illumination using a Keithley 2400 Source Meter in combination with a solar simulator (Enli Tech, Taiwan).

The time-resolved THz (TR-THz) spectroscopy was based on a regeneratively amplified Ti:sapphire laser system (800nm, 1 kHz repetition rate). An 800 nm beam was split into two branches for the THz generation and detection. The THz pulse was

generated via optical rectification of the 800 nm pulse in the ZnTe crystal. A high resistance Si wafer was placed after the ZnTe crystal to block the residual 800 nm beam and allow the THz to pass through. Then, the THz beam was collimated and focused onto the sample by off axis parabolic mirrors. The THz pulse transmitted through the sample was recollimated and focused into another ZnTe crystal for THz detection. In this ZnTe crystal, the THz propagates collinearly with the 800 nm probing beam. The time delay between the THz pulse and the 800 nm probing pulse was controlled by a motorized translation stage. Due to the electro-optic effect applied by the THz pulse, the polarization of the 800 nm probing pulse was rotated after passing through the ZnTe crystal, and the rotation was proportional to the electric field of THz. Then, the probing pulse was split into two beams with vertical and horizontal polarizations by a Wollaston prism and measured by a set of balanced diodes. The electric field of the THz pulse in time domain was recorded by varying the time delays between the THz pulse and the 800 nm probing pulse. The frequency range of the THz spectrum was 0.25-2 THz. The optical pump pulse was obtained via the second harmonic generation of the 500 nm pulse from a TOPAS optical parametric amplifier, and its repetition was chopped at frequency of 500 Hz by a chopper synchronized with the laser pulses. The delay between the THz and pump pulses was controlled by another motorized translation stage. The thickness of the film is around 500 nm.

Results

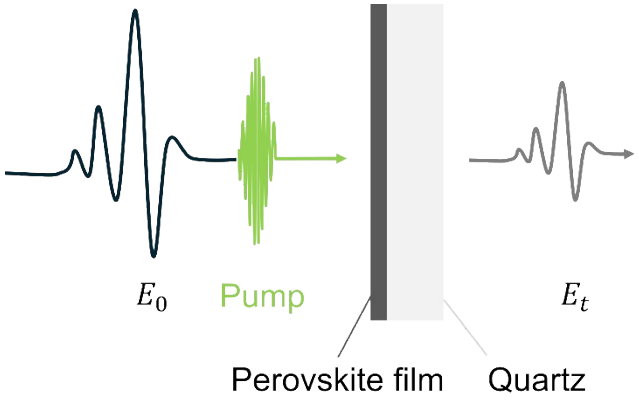

Figure S1. THz measurement schematic diagram. E_0 and E_t represent the time-domain spectra before and after passing through the sample, respectively, following optical excitation.

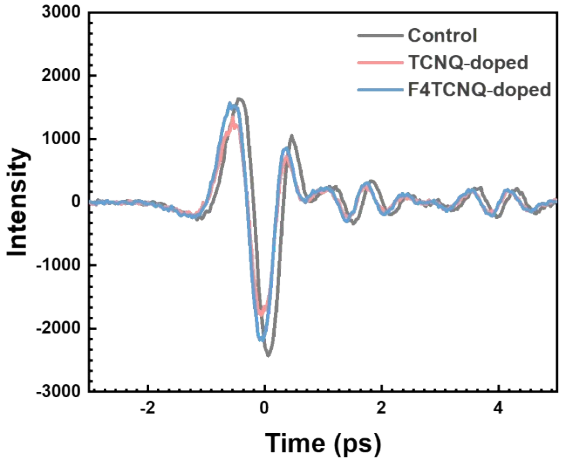

Figure S2. Waveforms of the photo-induced THz field change at indicated pump delays.

Table S1. List of fitting parameters for the fitting equation 1 in the main text. DC is dc conductivity.

Parameters / Samples	DC	τ (fs)	c	$\mu_h(cm^2 \cdot V^{-1} \cdot s^{-1})$
Control	81.42±2.02	87.68±4.48	-0.74±0.02	140.79±7.19
TCNQ-doped	56.99±1.52	85.55±5.09	-0.71±0.02	150.35±8.95
F4TCNQ-doped	71.71±1.60	96.25±4.47	-0.71±0.02	169.15±7.86

Table S2. Fitting parameters for TRPL of the control, TCNQ- and F4TCNQ-doped perovskite films.

	A1 (%)	τ_1 (ns)	A2 (%)	τ_2 (ns)	τ_{ave} (ns)
Control	58.6651	5.033	151.5695	54.82	53.1115
TCNQ-doped	134.1625	1.986	85.3256	35.59	32.8794
F4TCNQ-doped	126.3512	3.540	111.8933	38.50	35.2116

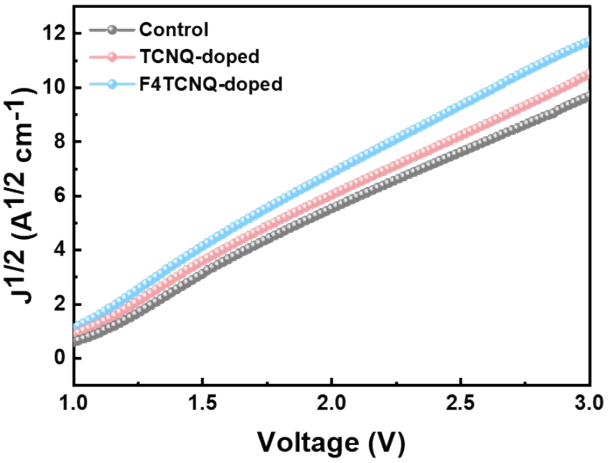

Figure S3. The $J^{1/2}$-V curve for the hole only devices.

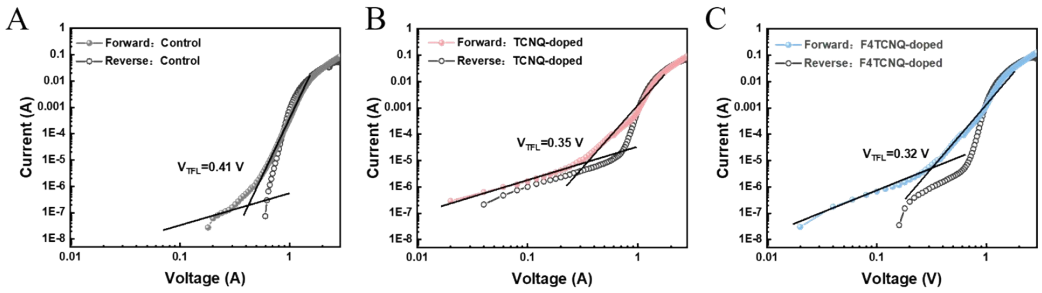

Figure S4. Current-voltage curves of the hole-only devices with or without molecule incorporated in perovskite film. A) Control, B) TCNQ-doped, C) F4TCNQ-doped.

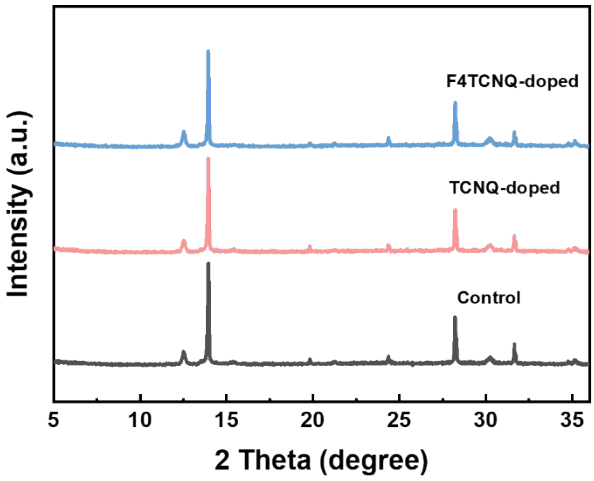

Figure S5. XRD patterns of the control, TCNQ- and F4TCNQ-doped perovskite films deposited on ITO.

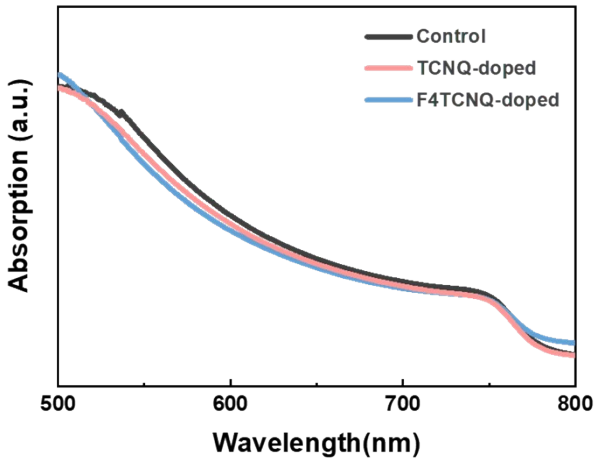

Figure S6. UV-vis absorption spectra of the control, TCNQ-d and F4TCNQ-doped perovskite films deposited on ITO.

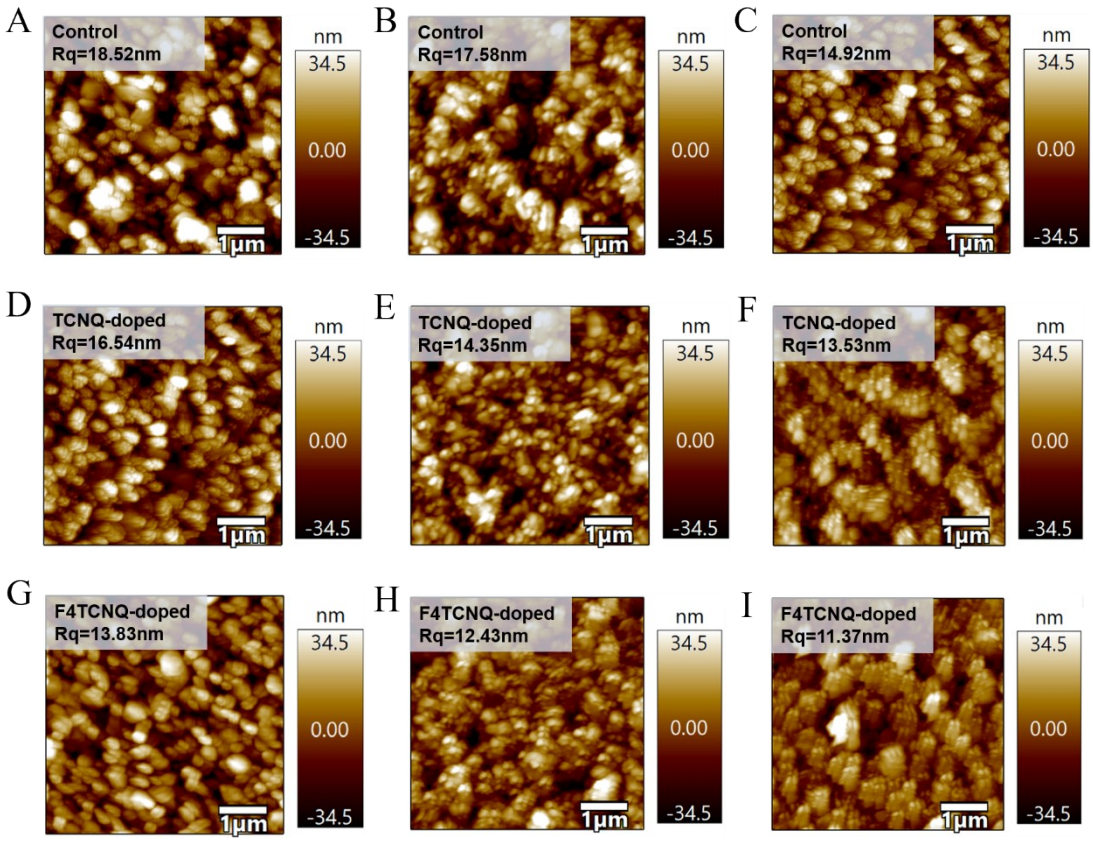

Figure S7. A-I) AFM images of the Control, TCNQ- and F4TCNQ-doped perovskite films deposited on ITO. The average roughness of the Control, TCNQ- and F4TCNQ-doped perovskite films are 17.01 nm, 14.81 nm, 12.54 nm respectively.

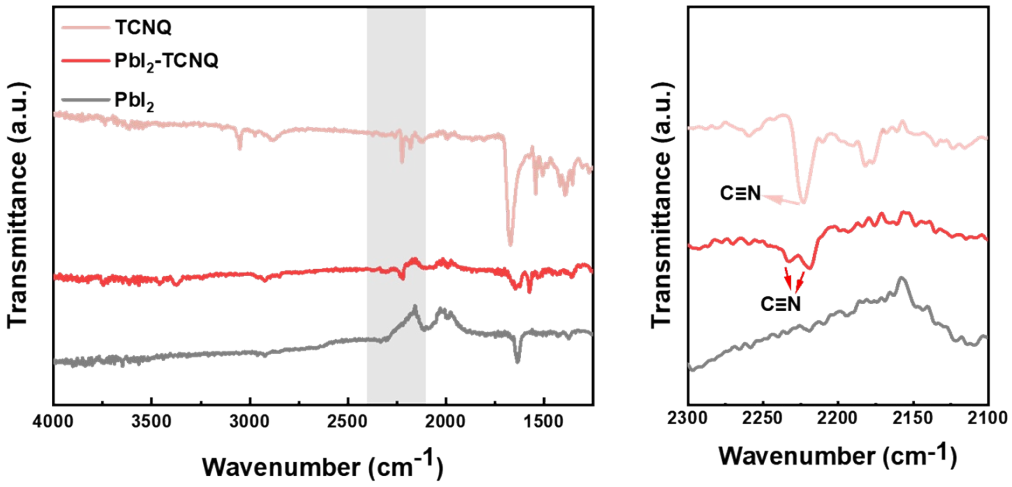

Figure S8. Fourier transform infrared (FTIR) spectroscopy of PbI_2, TCNQ and TCNQ-PbI_2 prepared by mixing F4TCNQ with PbI_2.

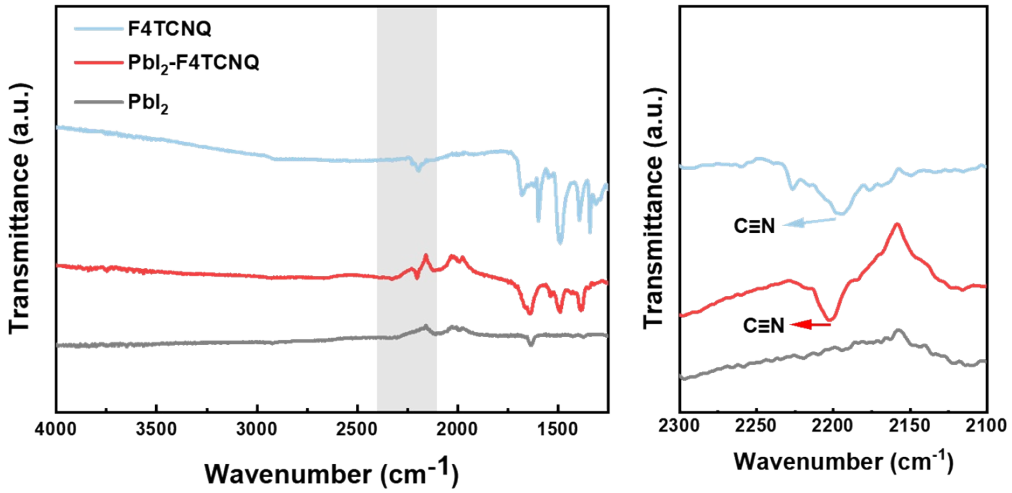

Figure S9. FTIR spectroscopy of PbI_2, F4TCNQ and F4TCNQ-PbI_2 prepared by mixing F4TCNQ with PbI_2.

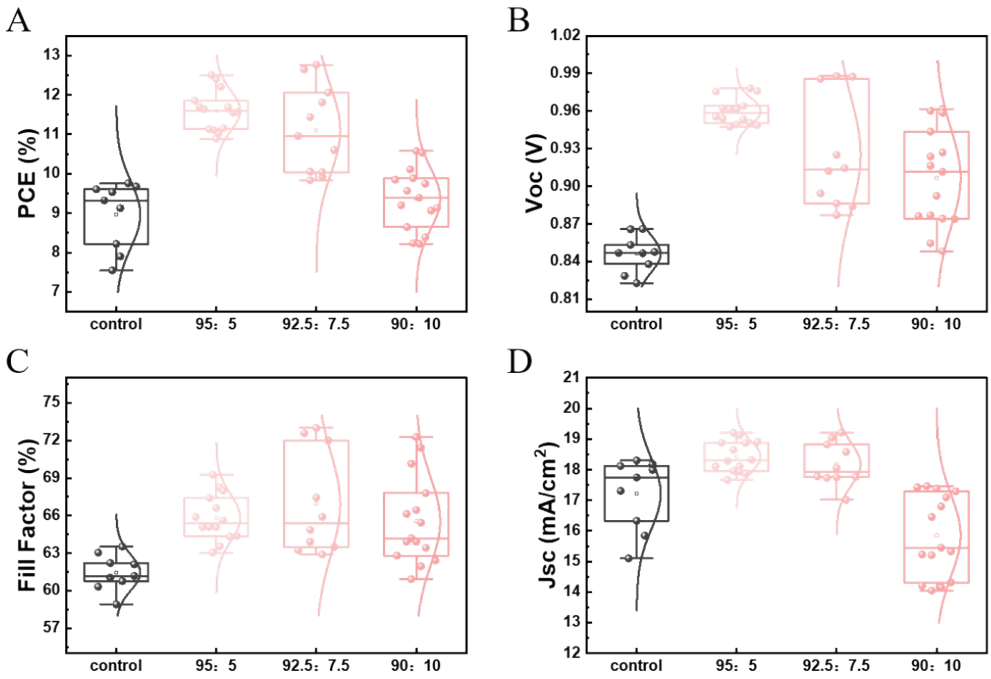

Figure S10. Statistic photovoltaic performance of devices based on TCNQ-doped perovskite film with different volume ratio. (perovskite solution: TCNQ volume ratio =95:5、92.5:7.5、90:10). (A) PCE, (B) V_{oc}, (C) fill factor, (D) J_{sc}.

Table S3. Average photovoltaic parameters of devices based on TCNQ-doped perovskite film with different volume ratio.

	PCE (%)	**V_{oc} (V)**	**Fill factor (%)**	**Jsc (mA/cm²)**
Control	8.96±0.86	0.84±0.01	61.44±1.42	17.21±1.17
95:5	11.60±0.51	0.95±0.01	65.81±1.84	18.42±0.50
92.5：7.5	11.22±1.07	0.92±0.04	66.92±4.10	18.17±0.70
90：10	9.36±0.77	0.90±0.03	65.54±3.48	15.85±1.32

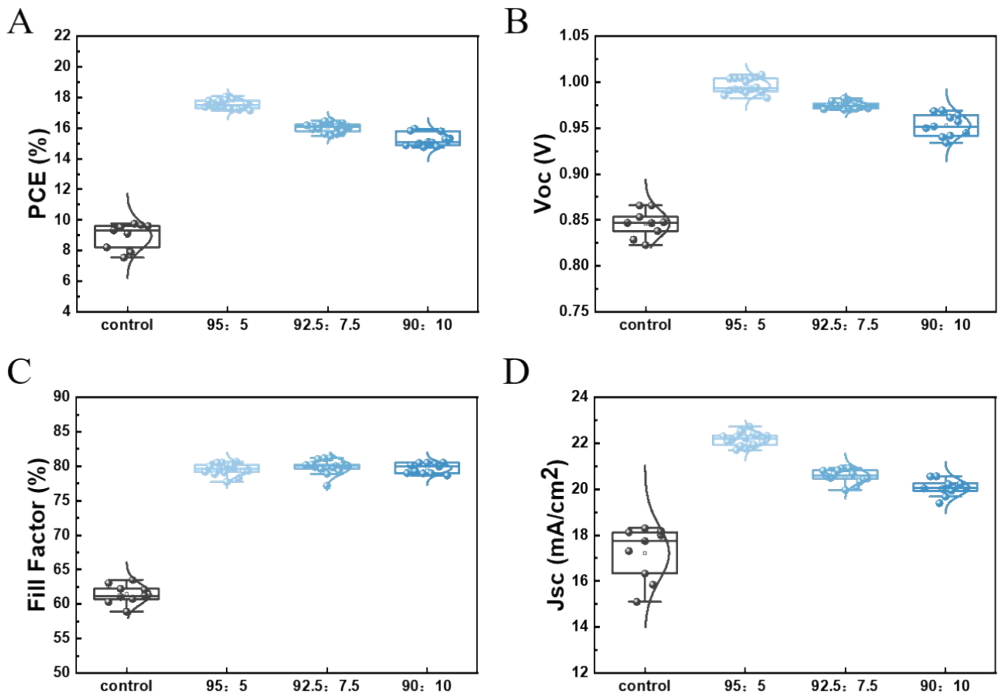

Figure S11. Statistic photovoltaic performance of devices based on F4TCNQ-doped perovskite film with volume ratio. (perovskite solution: F4TCNQ volume ratio =95:5, 92.5:7.5, 90:10). (A) PCE, (B) V_{oc}, (C) fill factor, (D) J_{sc}.

Table S4. Average photovoltaic parameters of devices based on F4TCNQ-doped perovskite film with different volume ratio.

	PCE (%)	**V_{oc} (V)**	**Fill factor (%)**	**J_{sc} (mA/cm^2)**
Control	8.96±0.86	0.84±0.01	61.44±1.42	17.21±1.17
95:5	17.56±0.30	0.99±0.01	79.54±0.82	22.16±0.28
92.5：7.5	16.01±0.31	0.97±0.01	79.90±1.03	20.57±0.30
90：10	15.24±0.43	0.95±0.01	79.70±0.74	20.06±0.34

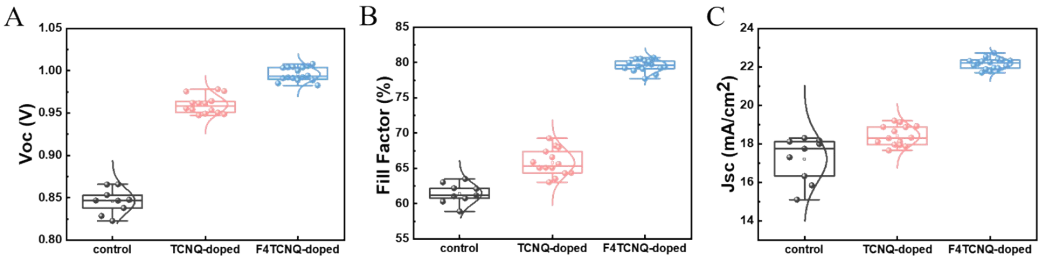

Figure S12. Statistic photovoltaic performance of devices based on the control, TCNQ- and F4TCNQ-doped perovskite films. (A) V_{oc}, (B) fill Factor, (C) J_{sc}.

Table S5. Average photovoltaic parameters of devices based on the control, TCNQ- and F4TCNQ-doped perovskite films.

	PCE (%)	**V_{oc} (V)**	**Fill factor (%)**	**J_{sc} (mA/cm^2)**
Control	8.96±0.86	0.84±0.01	61.44±1.42	17.21±1.17
TCNQ-doped	11.60±0.51	0.95±0.01	65.81±1.84	18.42±0.50
F4TCNQ-doped	17.56±0.30	0.99±0.01	79.54±0.82	22.16±0.28

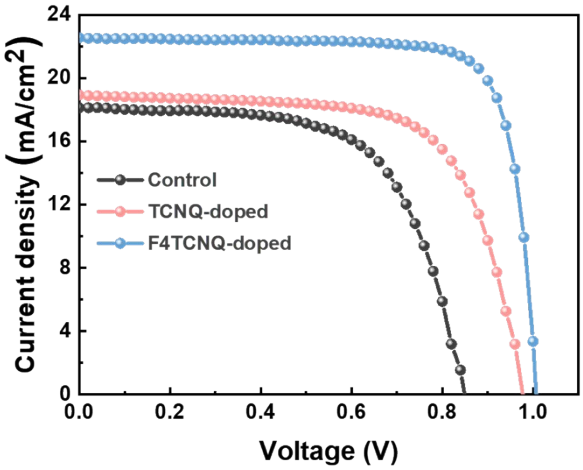

Figure S13. J-V characteristics of the champion devices based on the control, TCNQ- and F4TCNQ-doped perovskite films.

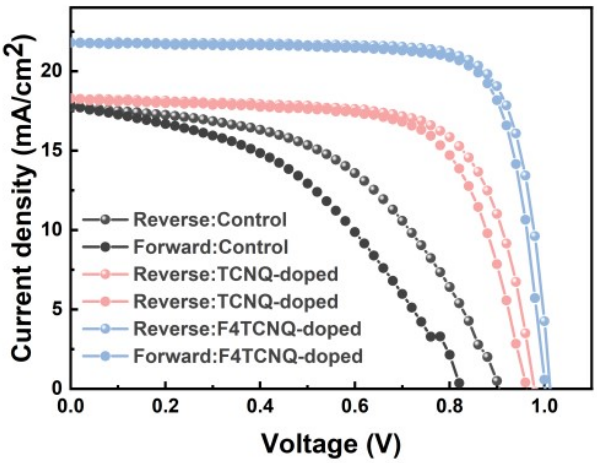

Figure S14. J-V curves with the reverse and forward scans of the devices based on the control, TCNQ- and F4TCNQ-doped perovskite films.

Table S6. The photovoltaic parameters extracted from the reverse and forward scans of the J-V curves.

		PCE (%)	V_{oc} (V)	Fill factor (%)	J_{sc} (mA/cm^2)	HI
Control	Reverse	8.14	0.903	50.77	17.74	0.206
	Forward	6.46	0.826	43.69	17.90	
TCNQ-doped	Reverse	12.66	0.978	70.88	18.26	0.048
	Forward	12.05	0.960	68.65	18.28	
F4TCNQ-doped	Reverse	17.45	1.010	79.31	21.79	0.022
	Forward	17.06	0.999	78.30	21.81	

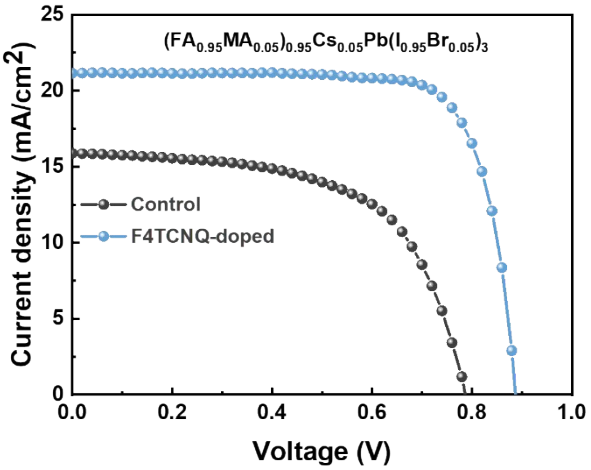

Figure S15. J-V characteristics of the optimized devices based on the Control and F4TCNQ-doped perovskite films. The perovskite is $FA_{0.9}MA_{0.03}Cs_{0.07}PbI_{2.76}Br_{0.24}$.

Table S7. Optimal photovoltaic parameters of the device based on the control and F4TCNQ-doped perovskite films. The perovskite is $FA_{0.9}MA_{0.03}Cs_{0.07}PbI_{2.76}Br_{0.24}$.

	PCE (%)	**V_{oc} (V)**	**Fill factor (%)**	**J_{sc} (mA/cm^2)**
Control	7.49715	0.78423	60.17226	15.88759
F4TCNQ-doped	14.43226	0.88485	77.10443	21.1536

Table S8. EIS impedance fitting parameters.

	Control	TCNQ-doped	F4TCNQ-doped
R_s (Ω)	14.200	6.294	6.759
R_{rec} (Ω)	4100	16500	30500
CPE (F)	$5.690X10^{-9}$	$9.983X10^{-9}$	$2.128X10^{-9}$
the non-ideality factor	0.93	0.85	0..89